Characterization of Metal−Cyanobacteria Sorption Reactions: A Combined Macroscopic and Infrared Spectroscopic Investigation

NATHAN YEE,*,[†,‡] LIANE G. BENNING,[†] VERNON R. PHOENIX,[‡] AND F. GRANT FERRIS[‡]

School of Earth Sciences, University of Leeds, Leeds LS2 9JT, United Kingdom and Department of Geology, University of Toronto, Toronto M5S 3B1, Canada

In this study, we conducted synchrotron radiation Fourier transform infrared (IR) spectroscopy, potentiometric titration, and metal sorption experiments to characterize metal−cyanobacteria sorption reactions. Infrared spectra were collected with samples in solution for intact cyanobacterial filaments and separated exopolymeric sheath material to examine the deprotonation reactions of cell surface functional groups. The infrared spectra of intact cells sequentially titrated from pH 3.2 to 6.5 display an increase in peak intensity and area at 1400 cm^{-1} corresponding to vibrational COO$^-$ frequencies from the formation of deprotonated carboxyl surface sites. Similarly, bulk acid−base titration of cyanobacterial filaments and sheath material indicates that the concentration of proton-active surface sites is higher on the cell wall compared to the overlying sheath. A three-site model provides an excellent fit to the titration curves of both intact cells and sheath material with corresponding pK_a values of 4.7 ± 0.4, 6.6 ± 0.2, 9.2 ± 0.3 and 4.8 ± 0.3, 6.5 ± 0.1, 8.7 ± 0.2, respectively. Finally, Cu^{2+}, Cd^{2+}, and Pb^{2+} sorption experiments were conducted as a function of pH, and a site-specific surface complexation model was used to describe the metal sorption data. The modeling indicates that metal ions are partitioned between the exopolymer sheath and cell wall and that the carboxyl groups on the cyanobacterial cell wall are the dominant sink for metals at near neutral pH. These results demonstrate that the cyanobacterial surfaces are complex structures which contain distinct surface layers, each with unique molecular functional groups and metal binding properties.

Introduction

Cyanobacteria are photosynthetic prokaryotes commonly found in soils, geothermal hot springs, freshwater, and saline lakes and are an important component of marine phytoplankton. Laboratory and field studies have shown that cyanobacteria are highly effective biological sorbents (e.g., *1−3*) and represent an important sink for metals in aquatic settings (*4−7*). Because of their strong affinity to bind dissolved metals, cyanobacteria can play an important role in affecting metal speciation (*8*) and heavy metal contaminant sequestration (*9−12*). To accurately predict the fate of metals in cyanobacteria-inhabited environments, a quantitative and mechanistic understanding of metal−cyanobacteria sorption reactions is needed. However, our current knowledge of metal uptake by cyanobacteria is largely empirical and limited by a lack of molecular-scale information.

The affinity for metal ions to bind onto cyanobacteria arises from the presence of proton-active surface carboxyl, phosphoryl, hydroxyl, and amine functional groups located on the cell wall and exopolymer sheath (*13*). These functional groups can deprotonate and bind metal ions to form stable ligand−metal surface complexes. Recent studies have applied chemical equilibrium surface complexation theory to describe metal sorption onto biological surfaces, including Gram-positive bacteria and Gram-negative bacteria (*14−20*). Because metal ions react with microbial surfaces to form complexes with different thermodynamic properties, site-specific metal binding models are required to accurately describe the sorption process. Surface complexation modeling explicitly accounts for the heterogeneous functionality of microbial surfaces by expressing specific stability constants for each metal−ligand surface complex. However, applying surface complexation theory to cyanobacteria requires a detailed understanding of the distribution and identity of cyanobacterial cell surface functional groups.

Previous investigations have used macroscopic acid−base titration and metal uptake experiments to characterize the reactivity of cell surface functional groups (e.g., *15*). Acid−base titration curves yield important information about the concentration and acidity of proton-active surface ligands, and metal sorption experiments provide quantitative constraints on the reaction stoichiometry and thermodynamic stability of metal−ligand surface complexes. However, acid−base titration and metal sorption experiments alone cannot be used to establish the identity of reactive surface ligands. Recent studies have indicated that spectroscopic techniques may be useful complimentary tools to study the molecular-scale processes that govern metal−bacteria sorption reactions (*21*, *22*).

IR spectroscopy is a well-established analytical technique which can be applied to determine the identity and protonation states of organic function groups (*23*). Each type of functional group has unique molecular vibration modes corresponding to specific infrared light frequencies. The composition and structure of molecular functional groups can be determined by analyzing the position, width, and intensity of infrared light absorption. Because infrared radiation is nondestructive to biological materials, it is can be used to examine the functional group chemistry of living cells and isolated cellular components (e.g., *24*). Furthermore, recent studies have demonstrated that synchrotron radiation-based IR microspectroscopy can achieve the spatial resolution to probe the molecular chemistry of single cells (*25−29*). Synchrotron radiation is 1000 times brighter than standard thermal infrared sources (*30*) and produces a high signal-to-noise ratio, allowing diffraction-limited spatial resolution (*31*, *32*) and the ability to measure infrared spectra with samples in solution. This approach provides a means to probe microbe−fluid interactions and to monitor protonation reactions of cyanobacterial functional groups in situ and in vivo.

The objective of this study was to determine the identity, abundance, and strength of metal binding sites on cyano-

* Corresponding author phone: (973) 353-5034; fax: (973) 353-1965; e-mail: nyee@andromeda.rutgers.edu.
† University of Leeds.
‡ University of Toronto.

bacterial surfaces. A combination of in situ infrared spectroscopy, potentiometic titration, and Cu^{2+}, Cd^{2+}, and Pb^{2+} sorption experiments were carried out on intact filaments and separated exopolymeric sheath material of the filamentous cyanobacteria *Calothrix* sp. strain KC97. The experimental data were used to (1) identify the dominant proton-active functional groups, (2) determine the concentration and acidity of surface sites on the *Calothrix* cell wall and exopolymer sheath, and (3) calculate the thermodynamic stability constants for each metal–ligand surface complex.

Materials and Methods

Growth and Preparation of Cell Culture. *Calothrix* is a filamentous organism commonly found in hot springs, lakes, soils, intertidal zones, sphagnum bogs, freshwater rivers, and marine environments *(33–36).* During growth, *Calothrix* forms trichomes up to 1 mm long that are surrounded by a thick polysaccharide sheath (up to 5 μm in thickness). In our experiments, *Calothrix* filaments were cultured in autoclaved liquid BG11 media under an average light irradiance of 700 lux. BG11 is composed of 1500 ppm $NaNO_3$, 40 ppm $K_2HPO_4 \cdot 3H_2O$, 75 ppm $MgSO_4 \cdot 7H_2O$, 36 ppm $CaCl_2 \cdot 2H_2O$, 6 ppm citric acid, 6 ppm ferric ammonium citrate, 1 ppm EDTA, 20 ppm Na_2CO_3, 2.9 ppm H_2BO_3, 1.8 ppm $MnCl_2 \cdot 4H_2O$, 0.2 ppm $ZnSO_4 \cdot 7H_2O$, 0.4 ppm $NaMoO_4 \cdot 2H_2O$, 0.08 ppm $CuSO_4 \cdot 5H_2O$, and 0.05 ppm $Co(NO_3)_2 \cdot 6H_2O$. After growing for 4 weeks, the colonies were homogenized in a tissue grinder with a Teflon pestle to break up clusters of filaments. The culture media was then removed by centrifugation, and the cells were rinsed 3 times in 250 mL of 0.01 NaCl electrolyte solution. Before experimentation, the filaments were examined with light microscopy to determine if the clusters were broken, but the cells remained intact.

Sheath material was separated from the cells by an extraction procedure based on Weckesser et al. *(37).* The *Calothrix* sp. filaments were rinsed in ultrapure water 3 times and then sonicated at an output frequency of 23 kHz and 6 μm amplitude for 30 cycles to disrupt the cells (each cycle was composed of 90 s of sonication and 30 s of cooling). The homogenate was then centrifuged at 10 000 rpm for 30 min, and the supernatant was removed. The pellet was resuspended in a 0.05 M HEPES buffer (pH 6.8) containing 200 mg/L lysozyme (chicken egg white variety) and incubated overnight at 37 °C. After incubation, sodium dodecyl sulfate (SDS) was added to the suspension (final SDS concentration 2% w/v) and boiled for 15 min. The suspension was then allowed to cool and rinsed 3 times with a 0.01 NaCl electrolyte solution. This separation procedure produced clear, colorless, and empty sheath material 3–5 μm in diameter, as determined by light microscopy.

Infrared Spectroscopy. Infrared spectra of intact cells and isolated sheaths were collected at the Advanced Light Source (Lawrence Berkeley National Laboratory) on the Infrared Beamline 1.4.3. The synchrotron light is incident onto a Nicolet Magna 760 FTIR bench and is passed through a Nicolet Nic-Plan IR microscope with a 10 × 10 μm upper aperture. The beamline has an incident infrared energy range of 0.05–1.0 eV, which is nondestructive to biologic materials. All infrared spectra were recorded in the mid-infrared range from 4000 to 650 cm^{-1}, which contains unique molecular fingerprint exhibiting vibrational frequencies of biomolecular functional groups. In this IR range, the ALS IR brightness is approximately 10^{12} photons/s·mm² mrad²·0.1% BW. For our infrared measurements, 512 spectra were collected at a spectral resolution of 8 cm^{-1} and co-added to enhance the signal-to-noise ratio. The spectra were collected in transmission and background corrected. All infrared spectra were carried out with samples in solution using a flow-through fluid cell.

A cell suspension of cyanobacteria was diluted with a 0.01 M NaCl electrolyte solution to a final optical density (OD) of 0.3 at 720 nm. A 5 μL drop of this suspension was placed in a flow cell between two infrared transparent windows (BaF_2 and ZnSe) separated by a Mylar spacer with a path length of 6 μm. The flow cell was connected to a peristaltic pump, and a 0.01 NaCl electrolyte solution flowed through the fluid cell at a constant flow rate. The pH of the input solution was adjusted to the desired pH using 0.1 M HCl and 0.1 M NaOH, and the pH of both the influent and effluent solutions was monitored continuously using microelectrodes. Once the pH of the output solution stabilized and reached the same pH value of the input solution (equilibrate time approximately 30 min), infrared spectra were collected for the sample. For each IR spectrum, a single filament of *Calothrix* was placed in front of the IR beam. IR spectra were recorded for the same cyanobacterial filament during the entire experiment. This approach eliminates the inherent scatter due to sample-to-sample variations and allows for detailed features of the spectral changes to be resolved. All infrared spectral characteristics were interpreted according to well-documented spectral research literature *(38–40).*

Potentiometric Titration and Metal Sorption Experiments. Acid–base titration experiments were conducted using an autotitrator assembly with either intact cyanobacteria cells or isolated sheath material suspended in a 20 mL of 0.01 M NaCl solution. The electrolyte used was purged of dissolved CO_2 by bubbling N_2 gas for 1 h, and the titration experiments were conducted in a N_2 atmosphere. The titrations were carried out using a commercially supplied volumetric standard of 1.0005 M HNO_3 and a carbonate-free 0.1058 M NaOH solution standardized against the acid. The pH sequence 'down–up' was chosen after tests revealed a higher tolerance of *Calothrix* to acid over base. A known amount of HNO_3 was added at the beginning of the experiment to lower the pH to approximately 3. The cell suspension was allowed to equilibrate for 30 min before titration with NaOH up to pH 10. At each titration step a stability of 0.1 mV/s was attained before the next aliquot of titrant was added. Before experimentation, aliquots of the cyanobacteria and sheath suspensions were used to determine the dry biomass. The dry mass was determined by filtration through a 0.2 μm pore size Supor filter and air dried at 70 °C to a constant weight. The uncertainty of the dry weight determination was ±2.3% (1σ). The dry mass of the sheath was determined to be approximately 18% of the total mass of the cell. The amount of cyanobacteria and sheath biomass used for the titration experiments ranged from 0.5 to 2 g/L and 0.1 to 0.4 g/L, respectively.

Metal sorption experiments were performed as a function of pH with Cu^{2+}, Cd^{2+}, and Pb^{2+}. A 50 μM amount of metal standard (Cu^{2+}, Cd^{2+}, or Pb^{2+}) was reacted with a known amount of cyanobacteria cells or isolated sheath material in a 0.01 M NaCl electrolyte solution. The pH of each batch experiment was adjusted to the desired value using 0.1 M NaOH or HNO_3 and allowed to equilibrate for 2 h. Each sample was subsequently filtered (0.45 μm), acidified to prevent precipitation, and analyzed for dissolved Cu, Cd, and Pb using an inductively coupled plasma–atomic emission spectroscopy (ICP-AES) technique. The amount of metal sorption was determined by calculating the difference between the initial metal concentration and metal concentration analyzed in the filtrate. All potentiometric titration and metal sorption experiments were performed in triplicate using independent *Calothrix* cultures.

Modeling Methods. We invoked a nonelectrostatic site-specific surface complexation model to describe the titration and metal sorption data. Proton dissociation from cell surface ligands can be described by the following reaction

$$HL^0 \leftrightarrow H^+ + L^- \tag{1}$$
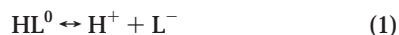
where L^- is the proton binding site on the cell and H^+ is a proton in solution. The total surface charge excess, $[L^-]_T$ (μmol/mg), was determined from the acid$-$base titration data. The total concentration of proton binding sites is equal to the difference between the total base added and the equilibrium H^+ and OH^- ion concentrations at any given point of the titration curve

$$[L^-]_T = C_a - C_b + [OH^-] - [H^+] \tag{2}$$

where C_a and C_b refer to the concentration of acid and base added, respectively. The concentration of protonated and deprotonated surface sites can be quantified with the corresponding mass action equation

$$K_a = \frac{[L^-][H^+]}{[HL^o]} \tag{3}$$

where K_a is the acidity constant. Because the proton binding ligands are heterogeneously distributed between the cell wall and exopolymer sheath, the location of reactive functional groups must be specified. The total concentration of surface ligands can be separated into two components

$$[L^-]_T = [\alpha\text{-}L^-] + [\beta\text{-}L^-] \tag{4}$$

where $[L^-]_T$ is the total ligand concentration, $[\alpha\text{-}L^-]$ is the ligand concentration on the exopolymer sheath, and $[\beta\text{-}L^-]$ is the ligand concentration on the cell wall. $[L^-]_T$ and $[\alpha\text{-}L^-]$ can be determined from the titration of intact cells and sheath material, respectively, and $[\beta\text{-}L^-]$ can be calculated from the difference between $[L^-]_{Total}$ and $[\alpha\text{-}L^-]$. The complexation of a metal ion with a surface ligand on the cell wall and sheath can be described with the following equilibrium reactions

$$\alpha\text{-}L^- + M^{m+} \leftrightarrow \alpha\text{-}L\text{-}M^{(m-1)+} \tag{5}$$

$$\beta\text{-}L^- + M^{m+} \leftrightarrow \beta\text{-}L\text{-}M^{(m-1)+} \tag{6}$$

where M^{m+} is the metal ion. log K values for reactions 5 and 6 were used to quantify the partitioning of metal between the surface and aqueous phase.

The concentration of surface ligands, log K_a values for the proton dissociation reactions, and log K values for the metal sorption reactions were calculated using the computer program FITEQL (41). The effects of aqueous complexation with Cl^-, CO_3^{2-}, and OH^- were accounted for in the calculations. The optimization procedure of FITEQL involves the iterative application of a linear approximation of the chemical equilibrium equation and a linear least-squares fit. An overall variance, $V(Y)$, is calculated between the model fit and experimental data, which provides a quantitative assessment of goodness of fit. For each data set, the number of surface sites and stability constants for each reaction can be adjusted until a best-fit curve is obtained. For systems containing a reactive surface, $V(Y) < 20$ indicates a good fit to the data. This approach has been used to describe similar proton and metal sorption reactions with bacterial surfaces in previous studies (e.g., 15$-$17, 19). An electrical double-layer model was not used to correct for the effects of bacterial surface electric field, and therefore, the log K values should be regarded as apparent equilibrium constants conditional to the solution ionic strength, $I = 0.01$ M, and is valid only at low metal loading on the cell surface.

Results and Discussion

Infrared Spectroscopy. Figure 1a displays the infrared spectra of an intact *Calothrix* sp. filament in a 0.01 M NaCl electrolyte
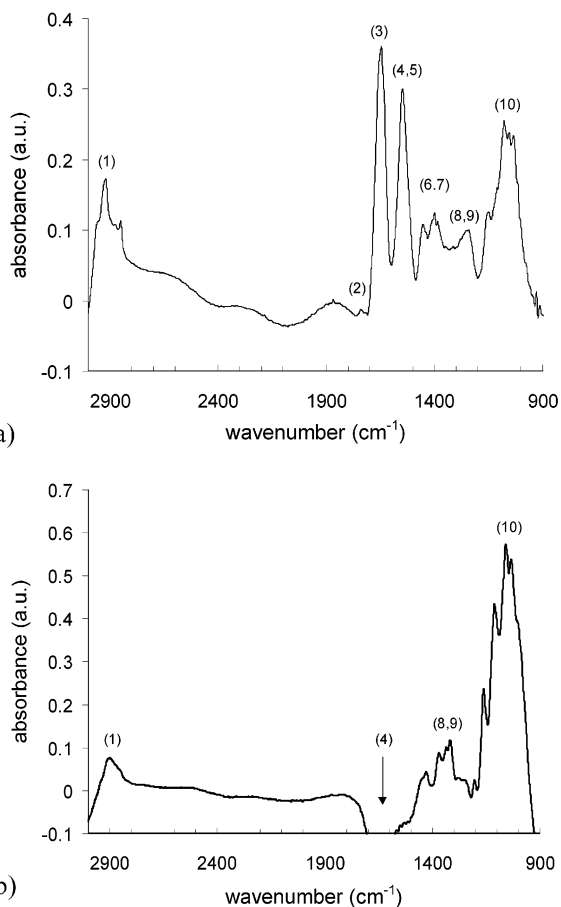

(a)

(b)

FIGURE 1. Infrared spectra of *Calothrix* collected in 0.01 NaCl electrolyte solution of (a) an intact filament at pH 6.3 and (b) isolated exopolymer sheath at pH 8.2. See Table 1 for specific band assignments.

solution at pH 6.3. The infrared bands are composed of a combination of protein, lipid, and carbohydrate functional group peaks. The spectral features for bacteria are well established (39, 40), and the infrared band assignments for *Calothrix* have been recently assigned by Benning et al. (29). The cyanobacterial functional groups and corresponding infrared frequencies are summarized in Table 1. At 1646 and 1548 cm^{-1}, the amide I and amide II bands were observed, respectively. The region between 3000 and 2800 cm^{-1} exhibits the C$-$H stretching vibrations of $-CH_3$ and $>CH_2$ functional groups attributed to fatty acids found in membrane phospholipids. Complimentary information can be deduced from the bands between 1470 and 1300 cm^{-1}, where the deformation modes of C$-$H, $-CH_3$, and $>CH_2$ functional groups were observed. The membrane phospholipids also contain ester functional groups, which form a characteristic peak at 1741 cm^{-1} due to the vibrational C$=$O stretching frequencies. Additional information on phospholipids along with phosphodiesters, free phosphate, and monoester phosphate functional groups can be determined in the region between 1250 and 1200 cm^{-1}, which correspond to $>P=O$ double-bond asymmetric stretching frequencies. The $>P=O$ phosphodiester functional groups also contribute to spectral features in this region. The bands between 1200 and 900 cm^{-1} are dominated by a sequence of peaks due to C$-O-C$ and C$-O-P$ stretching vibrations of polysaccharides. Because of the complex superpositions of the characteristic absorption of various cellular polysaccharides, specific assignments are difficult.

The infrared spectra of an isolated *Calothrix* sheath were also collected in 0.01 M NaCl electrolyte solution at pH 8.2

TABLE 1. Cyanobacterial Functional Groups and Corresponding Infrared Absorption frequencies

IR band	frequency (cm⁻¹)[a]	functional group assignment[b]
1	3000-2800	Stretching of C-H, −CH₃, and >CH₂ functional groups
2	1700	ν C=O of COOH
3	1646	amide I band
4	1595	δ O-H vibrations
5	1548	amide II band
6	1470-1300	deformation of C-H, −CH₃, and >CH₂ functional groups
7	1400	ν_s C=O of COO⁻
8	1260	ν C-O of COOH
9	1250-1200	ν_a PO₂⁻ stretching of phosphodiesters, free phosphate, or monoester phosphate functional groups
10	1200-900	C-O-C, C-O-P, P-O-P ring vibrations of polysaccharides

[a] Lin-vein et al. (38); Naumann et al. (39); Naumann (40). [b] ν_s = symmetric stretching; ν_a = asymmetric stretching; δ = bending.

(Figure 1b). The spectra show strong absorption bands in the region between 1200 and 900 cm⁻¹, with four distinct polysaccharide peaks at 1165, 1114, 1063, and 1050 cm⁻¹. The spectra also display peaks resulting from the stretching and deformation of C−H bonds between 3000 and 2800 cm⁻¹ and 1470−1300 cm⁻¹, respectively. In contrast to the intact *Calothrix* cells, the sheath material do not show the distinct amide I and II bands. Instead, we observed a dip in the infrared spectra between 1700 and 1550 cm⁻¹ (corresponding to O−H bending frequencies) resulting from the background solution correction. This water correction feature was noted for all spectra collected at the region near 1600 cm⁻¹ and in some cases overlap with the amide II peak (e.g., Figure 1a).

Figure 2a shows a series of infrared spectra collected for an intact *Calothrix* sp. filament that was sequentially titrated from pH 3.2 to 6.5. The results indicate that at low pH values, the spectra features are very similar, and no changes in the position, width, and intensity of characteristic functional group peaks were measured. However, as the pH increases, the infrared spectra display a distinct change in peak position from 1385 to 1400 cm⁻¹. From pH 4.3 to 6.5, we observed an increase in peak intensity and peak area at 1400 cm⁻¹ characteristic of symmetric vibrational (ν_s) COO⁻ frequencies of amino acid side chains and free fatty acids. Conversely, the infrared spectra collected for the isolated sheath from pH 3.6 to 9.3 do not show a change in peak intensity at 1400 cm⁻¹ or a shift in peak position (Figure 2b).

The protonation state of cell surface carboxyl functional groups is strongly pH dependent. In acidic solutions, protons can strongly bind onto surface functional groups and the dominant speciation of the carboxyl sites is the protonated form (−COOH). From pH 3.2 to 4.3, minimal changes in molecular vibrations of the functional groups were observed, indicating that carboxyl group deprotonation does not occur. As the pH increases, the chemical driving force for proton desorption increases, resulting in the progressive formation of deprotonated carboxylic surface sites. This deprotonation reaction was observed by the increase in the vibrational frequencies of COO⁻ groups at 1400 cm⁻¹ (ν_s COO⁻) from pH 4.3 to 6.5.

Carboxyl groups within the *Calothrix* cell wall are found in the outer membrane and peptidoglycan layers. In the outer membrane, carboxyl groups are located in the β-hydroxy-palmitic acid and ketodeoxyoctate moieties of the lipopolysaccharide (42, 43). In peptidoglycan layer, carboxyl groups are contained in the peptide cross-linkages (alanine, glutamic acid, lysine, and diaminopimelic acid). Although the cell wall of cyanobacteria is Gram-negative in structure, it contains a thick layer of peptidoglycan and a high degree of peptide cross linkages similar to Gram-positive bacteria (44). The unlinked peptide cross-links of peptidoglycan represent the dominant source of reactive carboxyl groups on the surfaces of both Gram-positive and Gram-negative
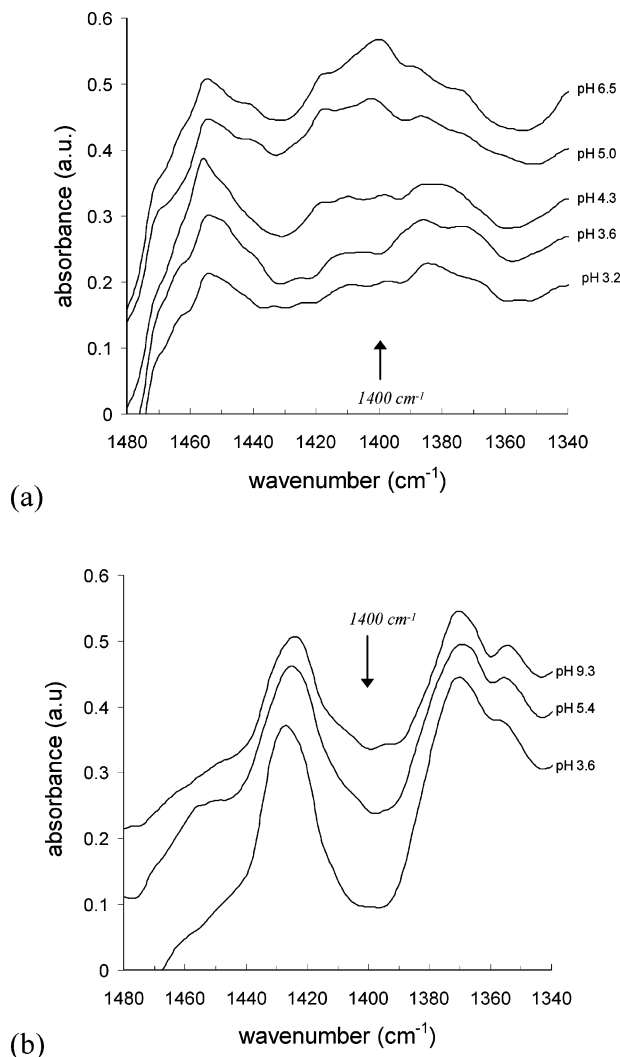

(a)

(b)

FIGURE 2. Infrared spectra collected as a function of solution pH for (a) an intact *Calothrix* filament from pH 3.2 to 6.5 and (b) isolated sheath material from pH 3.6 to 9.3.

bacteria (45−47). Because peptidoglycan is found in all bacteria species, this reactive surface structure is common to all bacteria types.

The formation of deprotonated carboxyl functional groups was not detected in the infrared spectra of the isolated sheath (Figure 2b). No spectral changes were observed at the 1400 cm⁻¹ region over a wide pH range, suggesting that proton-active carboxyl groups are largely located in the cell wall and not in the exopolymer material. The exopolymer sheath is composed of the neutral sugar compounds galactose and

glucose, with minor amounts of mannose, xylose, arabinose, rhamnose, fucose, and two O-methyl sugars (*37*). Previous bioassay studies have determined the presence of galacturonic acid in certain cyanobacterial sheaths (*37, 48*), which is a potential source of reactive carboxylic groups in the extracellular polysaccharides. However, galacturonic acid occurs only in trace amounts, and it is probable that the concentration of proton-active carboxyl functional groups in the sheath is below the detection limit of our infrared spectroscopic approach.

Spectroscopic examination of the intact cells and isolated exopolymer material suggests that the presence and identity of reactive functional groups are unique to certain surface layers. In contrast to mineral surfaces, the surfaces of microorganisms contain multiple reactive layers, each with a distinct structure and chemical composition. The distribution of functional groups between the various layers likely reflects the different biological functions of each cell wall component. Because the cell wall is a complex three-dimensional structure, two-dimensional surface complexation models are not directly applicable to microorganisms. To accurately describe metal−cyanobacteria sorption reactions, the distribution and identity of functional groups between the various surface components must be established.

Infrared spectra for both intact cells and isolated sheath material show an increase in peak intensity at around 1235 cm^{-1} which may be attributable to PO$_2^-$ asymmetric stretching vibrations (data not shown). Symmetry variations associated with metal or organic molecule complexation produce spectral features at around 1200 cm^{-1}. However, phosphate groups linked to organic molecules may exhibit only limited variation in its structure and symmetry from changes in its protonation state. Furthermore, the protonated forms of carboxylic groups also show features around the same infrared frequencies and may interfere with those of phosphate groups. Alternatively, deprotonation reactions of phosphoryl groups could have been detected at vibration frequencies of phosphate groups that occur below 1020 cm^{-1}. However, spectral changes at these infrared frequencies could not be measured due to diffraction limitations of the infrared beam caused by the size of the aperture used in the experiments (e.g., *25*).

Variations in spectral features attributable to the deprotonation of amine and hydroxyl functional groups were not observed. The IR spectra recorded from pH 3.3 to 9.6 for intact cells and pH 3.6 to 9.3 for isolated sheath material do not show changes in characteristic amino peaks positions, e.g., N−H stretching at 3030 cm^{-1} and N−H bending at 1540 cm^{-1} (data not shown). Amino acids strongly absorb infrared light, but proton-active amine groups on the cell surface represent only a small fraction of the total proteins of the cell. Therefore, IR absorption of proteins within the cell dominants over any changes in the molecular vibrations from the cell wall/sheath amine groups. Furthermore, the characteristic hydroxyl functional group peak positions of common biomolecules (e.g., symmetric O−H stretching at 3500 cm^{-1}) occur in the same range as the molecular vibrations of H$_2$O and therefore could not be detected due to interference with the background solution.

Potentiometric Titration Experiments. Figure 3 is a plot of the acid−base titration curves collected for intact *Calothrix* cells and isolated sheath material. The intact cyanobacterial filaments show significant surface charge excess across the pH range studied. In contrast, the isolated sheath material displays a very weak buffering effect indicating that the total concentration of proton-active functional groups on the sheath is much lower compared to the cell wall. A Student's *t*-test was used to determine if the site concentrations between the intact cells and isolated sheaths are significantly different. The analysis of the triplicate titration experiments
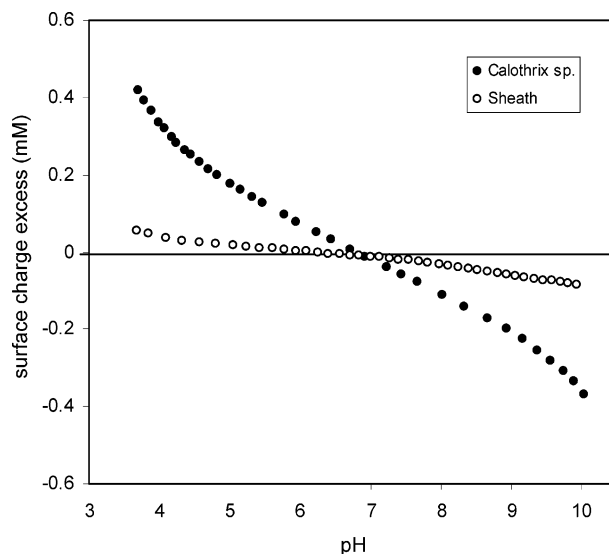

FIGURE 3. Surface charge excess plots for intact *Calothrix* cells and isolated sheath material.

TABLE 2. Concentration and Acidity Constants for Surface Functional Groups of *Calothrix*

surface component	suggested functional group	pK_a[a]	total site concentration[b]
sheath	α-carboxyl[c]	4.8 ± 0.3	0.46 ± 0.17
	α-phosphoryl	6.5 ± 0.1	0.45 ± 0.09
	α-amine	8.7 ± 0.2	0.92 ± 0.22
cell wall	β-carboxyl[d]	4.7 ± 0.4	3.28 ± 0.27
	β-phosphoryl	6.6 ± 0.2	4.15 ± 0.31
	β-amine	9.1 ± 0.3	7.16 ± 0.97

[a] Average apparent acidity constant conditional to I = 0.01 M and corresponding 1σ error. [b] Site concentration in 10^{-4} mol/g normalized to dry wt of cyanobacteria. [c] α indicates the functional group is attached to the sheath. [d] β indicates that the functional group is attached to the cell wall.

of the intact cells and sheath material showed the sites concentrations to be different at a confidence interval of 99%. We describe the proton binding behavior of the sheath material and intact cells using a nonelectrostatic discrete site model. Analysis of the titration data between pH 3 and 10 indicates that a three-site model provides the best fit for both the sheath and intact cells. The acidity constants and site concentrations for each type of surface functional groups are summarized in Table 2. $V(Y)$ values for the three-site model range from 18 to less than 1, indicating good to excellent fits to the experimental data. In contrast, $V(Y)$ values for two-site models are generally greater than 20. Additional proton binding sites in that pH range do not improve the fit to the titration curve. However, it should be noted that the model fit is not unique and does not provide unequivocal information about the molecular-scale mechanisms responsible for proton binding on the microbial cell surface. Different acid−base titration regression methods can yield equally good fits to bacteria titration data with varying number of surface sites (e.g., *15, 49*). Therefore, it is possible that the proposed three-site model only provides constraints on the acidity and site density of the dominant proton-active functional groups on the *Calothrix* surface.

By combining the IR data, cell wall biochemistry, and comparisons of pK_a values of functional groups attached to model compounds, tentative assignments of functional group identity can be made. On the sheath, we hypothesize the presence of carboxyl groups (pK_a of 4.8 ± 0.3), phosphoryl groups (pK_a of 6.5 ± 0.1), and amine groups (pK_a of 8.7 ± 0.2).
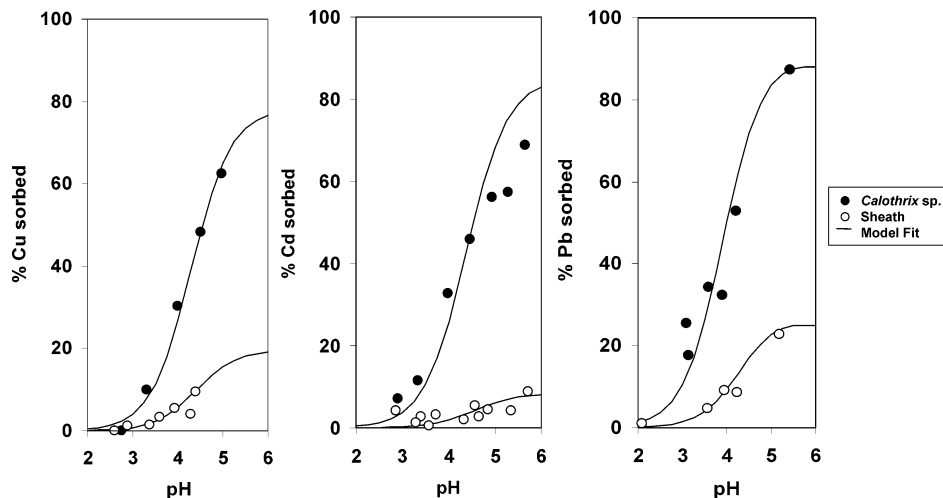
FIGURE 4. Cu, Cd, and Pb sorption onto *Calothrix* cells and isolated sheath material as a function of pH. The curves represent the best-fitting surface complexation model. The model fits were determined using the reactions and parameters in Table 3.

Similarly, on the cell wall we hypothesize the presence of carboxyl groups (pK_a of 4.7 ± 0.4), phosphoryl groups (pK_a 6.6 ± 0.2), and amine groups (pK_a of 9.1 ± 0.3). This functional group assignment is consistent with that proposed by Phoenix et al. (*13*) for proton binding sites on the *Calothrix* surface.

The IR data provides direct evidence for the presence of carboxyl groups on the cell wall. In the pH range that β-carboxyl groups become proton active, a distinct change in the infrared spectra at 1400 cm^{-1} was observed. The acidity constants are consistent with typical deprotonation constants for short-chained carboxylic acids ($4 < pK_a < 6$) (*50*). The titration data indicate that there are over 7 times more proton-active carboxylic groups located on the cell wall (3.28×10^{-5} mol/g) compared to the sheath (4.6×10^{-6} mol/g). The lower concentration of proton-active carboxyl groups on the sheath may explain the lack of spectral changes observed in IR spectroscopic measurements of the sheath material.

The IR data does not provide clear evidence for reactive phosphoryl, hydroxyl, and amine groups. However, phosphates are found in the cyanobacterial sheath, and a high concentration of phosphoryl groups are bound to the lipopolysaccharide, lipids, and muramic acid in the peptidoglycan. Amine groups are also present on the cyanobacterial surface and are associated with membrane proteins and the peptide component of peptidoglycan. Biochemical analysis has shown that amino acids are also present in the *Calothrix* sheath (*37*). On simple molecules, amine groups typically exhibit pK_a values between 8 and 11 (*50*). On the basis of similarities of pK_a values, Phoenix et al. (*13*) assigned the proton-active surface site in this pK_a range as an amine group. The protonated form of amine groups is the only type of surface site to display positive charge, and therefore, the detection of these functional groups has important implications for surface charge formation and the uptake of anionic metal complexes. It is possible that proton-active hydroxyl groups are also present on the cyanobacterial surface. High concentrations of hydroxyl groups are found in the polysaccharide compounds which make up the sheath and cell wall surface layers, but deprotonation of hydroxyl surface sites could not be observed due to interference with the background solution. Estimates for the pK_a value of bacterial surface hydroxyl group have ranged from 9.4 to 10.2 (*15, 16*); however, it remains unclear if surface hydroxyl groups participate in deprotonation or metal sorption reactions.

Metal Sorption Experiments. The results of Cd, Cu, and Pb sorption experiments are displayed in Figure 4. High amounts of metal uptake were measured for intact cells, and the affinity sequence Cd^{2+} < Cu^{2+} < Pb^{2+} was observed. The

TABLE 3. Surface Complexation Reactions and Model Parameters Describing Cu, Cd, and Pb Sorption onto *Calothrix*

metal	surface component	reaction[a]	log K[b]
Cu	sheath	α-COO$^-$ + Cu^{2+} $\leftrightarrow$ α-COO-Cu$^+$	4.31 ± 0.54
	cell wall	β-COO$^-$ + Cu^{2+} $\leftrightarrow$ β-COO-Cu$^+$	4.80 ± 0.71
Cd	sheath	α-COO$^-$ + Cd^{2+} $\leftrightarrow$ α-COO-Cd$^+$	3.38 ± 0.30
	cell wall	β-COO$^-$ + Cd^{2+} $\leftrightarrow$ β-COO-Cd$^+$	3.96 ± 0.32
Pb	sheath	α-COO$^-$ + Pb^{2+} $\leftrightarrow$ α-COO-Pb$^+$	5.07 ± 1.11
	cell wall	β-COO$^-$ + Pb^{2+} $\leftrightarrow$ β-COO-Pb$^+$	4.67 ± 0.08

[a] Metal sorption reaction onto surface sites locate on the cyanobacterial sheath (α) and cell wall (β). [b] Logarithm of the apparent stability constant conditional to $I = 0.01$ M can corresponding 1 σ error.

sheath material displayed a lower metal sorption capacity compared to the intact cyanobacterial filaments. This result suggests that metals ion are dominantly bound to cell wall functional groups with lower concentrations of the metal bound to functional groups on the sheath. Both the intact cells and isolated sheath display strong pH-dependent sorption behavior. The extent of sorption increased with increasing pH, corresponding to the progressive deprotonation of surface functional groups.

A one-site sorption model provides an excellent fit for metal−sheath sorption data. Metal sorption onto deprotonated α-carboxyl sites is the only mechanism that can reasonably explain the pH dependence sorption behavior observed. Models involving metal sorption onto phosphoryl or amine sites offer poor fits to the sorption isotherms. Furthermore, including a second site for the sorption reaction does not improve the fit of the model to the data and therefore is not warranted. However, the metal sorption experiments were conducted in narrow pH range (pH 2 to 6), and at higher pH conditions, metal complexation onto phosphoryl sites may become important. The log K values for Cu^{2+}, Cd^{2+}, and Pb^{2+} sorption onto α-carboxyl sites are 4.31 ± 0.54, 3.38 ± 0.30, 5.07 ± 1.11 (Table 3).

Intact cyanobacterial filaments sorbed significantly more metal than the sheath material. Because cyanobacterial surfaces are permeable three-dimensional structures, metal ions can readily react with ligands onto both the sheath and cell wall. The distribution of sorbed species between each surface layer component can be quantified by expressing an equilibrium equation for each metal−ligand complexation reaction. In addition to the metal binding sites on the sheath, a reactive site on the cyanobacterial cell wall are needed to
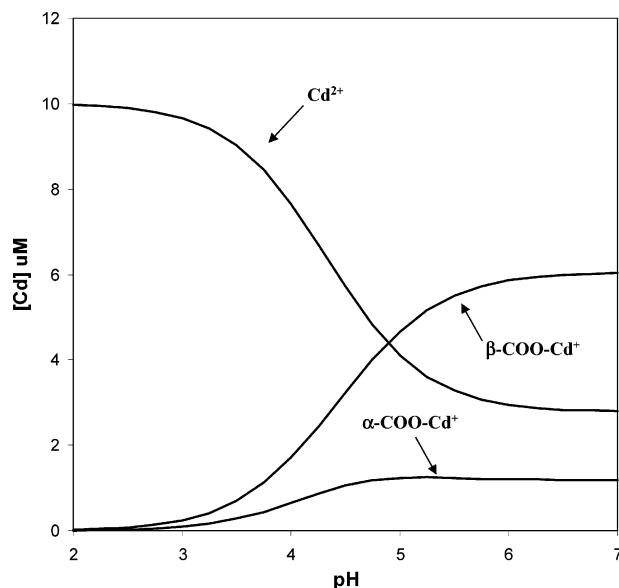
FIGURE 5. Calculated speciation of Cd^{2+} as a function of pH with 10 μM of Cd^{2+} exposed to 100 mg/L of cyanobacteria.

fit the metal sorption data with intact cyanobacterial cells. Table 3 lists the metal binding reactions onto sheath and cell wall bound ligands. The difference in metal binding between the isolated sheath material and intact cells can be accounted for by metal complexation onto deprotonated β-carboxyl sites. The strong pH-dependent sorption behavior is accurately described by metal binding onto carboxyl site on the *Calothrix* cell wall. log K values for Cu^{2+}, Cd^{2+}, and Pb^{2+} sorption onto β-carboxyl groups are 4.80 ± 0.17, 3.96 ± 0.32, 4.67 ± 0.08, respectively (Table 3). It is interesting to point out that the stability constant for the Cd−carboxyl cell wall complex is in excellent agreement with Yee and Fein (*19*), who reported a generalized log K value of 4.0 for Cd^{2+} sorption onto bacterial surfaces. This result suggests that cyanobacterial metal adsorption conforms to the universal adsorption edge hypothesis.

Using the mechanistic and quantitative constraints provided by infrared spectroscopy, potentiometric titration, and metal sorption experiments, the distribution of metal between various surface ligands can be estimated. Model parameters generated from fitting metal sorption can be directly incorporated into geochemical codes to predict the effect of metal−cyanobacteria sorption on metal speciation. To illustrate the utility of this approach, the speciation of Cd^{2+} exposed to 100 mg/L of cyanobacterial cells was calculated using the surface complexation reactions and model parameters in Table 3 (Figure 5). The calculation shows that at low pH, Cd^{2+} exists dominantly in the aqueous from as a free ion. As the pH increases, the concentration of free Cd^{2+} decreases and the metal is partitioned between the carboxyl sites on the sheath and cell wall (e.g., α-carboxyl and β-carboxyl groups). In agreement with the infrared spectroscopic data, the surface speciation model indicates that the carboxyl groups on the cyanobacterial cell wall are the dominant reactive sites on the cell surface and represent the most important sink for metal ions at near neutral pH.

The results of this study demonstrate that the reactive sites on *Calothrix* surfaces are heterogeneously distributed between the exopolymer sheath and cell wall. This dual-layer surface reactivity displayed by *Calothrix* may be a common feature among ensheathed cyanobacterial species. Cyanobacteria share very similar cell wall structures, and many cyanobacterial species surround their cell walls with a polysaccharide sheath (*34*). Although the sheath compositions have been analyzed for only a small number of cyanobacteria, the dominance of neutral sugars, reported in the sheath of *Calothrix* (*33*), has been documented for other cyanobacterial species (*51*, *52*). Therefore, the cell surface structure and composition of *Calothrix* bears similarities with a notable number of other cyanobacteria. However, variability in the relative concentration of surface sites may exist among different cyanobacteria species depending on the thickness of the sheath as well as metabolic state, growth phase, and growth conditions. These variations will affect the cell surface reactivity and ultimately the macroscopic metal sorption behavior. To account for these variations, an accurate knowledge of the concentration and distribution of cell surface functional groups is required. The advantage of a site-specific surface complexation approach is that changes in the relative concentration of surface sites can be readily incorporated into the surface speciation model to predict the macroscopic sorption isotherm. Such flexibility provides a means to accurately describe complex sorption phenomena in natural systems.

Acknowledgments

Literature Cited

(1) Pirszel, J.; Pawlik, B.; Skowronski, T. *J. Indus. Microbiol.* **1995**, *14*, 319.
(2) Blanco, A.; Sanz, B.; Llama, M. J.; Serra, J. L. *J. Biotechnol.* **1999**, *69*, 227.
(3) Prasad, B. B.; Pandey, U. C. *World J. Microbiol. Biotechnol.* **2000**, *16*, 819.
(4) Siggs, L. Metal transfer mechanisms in lakes; the role of settling particles. In *Chemical Processes in Lakes;* Stumm, W., Ed.; Wiley: New York, 1985.
(5) Siggs, L.; Sturm, M.; Kistler, D. *Limnol. Oceanogr.* **1987**, *32*, 112.
(6) Shafer, M. M.; Armstrong, D. E. Trace element cycling in southern Lake Michigan: role of column particle components. In *Organic Substances and Sediments in Water;* Baker, R. A., Eds.; Lewis: Chelsea, MI, 1991.
(7) Koelmans, A. A.; Gillissen, F.; Lijklema, L. *Water Res.* **1996**, *30*, 853.
(8) Croot, P. L.; Karlson, B.; Wulff, A.; Linares, F.; Anderson, K. *J. Mar. Syst.* **2002**, *35*, 39.
(9) Mohamed, Z. A. *Water Res.* **2001**, *35*, 4405.
(10) El-Enany, A. E.; Issa, A. A. *Environ. Toxicol. Pharmacol.* **2000**, *8*, 95.
(11) Matsunaga, T.; Takeyama, H.; Nakao, T.; Yamazawa, A. *J. Biotechol.* **1999**, *70*, 33.
(12) Rangsayatorn, N.; Upatham, E. S.; Kruatrachue, M.; Pokethitiyook, P.; Lanza, G. R. *Environ. Pollut.* **2002**, *119*, 45.
(13) Phoenix, V. R.; Martinez, R. E.; Konhauser, K. O.; Ferris, F. G. *Appl. Environ. Microbiol.* **2002**, *68*, 4827.
(14) Plette, A. C. C.; Benedetti, M. F.; Van Reimsdijk, W. H. *Environ. Sci. Technol.* **1996**, *30*, 1902.
(15) Fein, J. B.; Daughney, C. J.; Yee, N.; Davis, T. A. *Geochim. Cosmochim. Acta* **1997**, *61*, 3319.
(16) Daughney, C. J.; Fein, J. B.; Yee, N. *Chem. Geol.* **1998**, *144*, 161.
(17) Fowle, D. A.; Fein, J. B.; Martin, A. M. *Environ. Sci. Technol.* **2000**, *34*, 3737.
(18) Pagnanelli, F.; Papini, M. P.; Toro, L.; Trifoni, M.; Veglio, F. *Environ. Sci. Technol.* **2000**, *34*, 2773.
(19) Yee, N.; Fein, J. B. *Geochim. Cosmochim. Acta* **2001**, *65*, 2037.
(20) Martinez, R. E.; Ferris, F. G. *J. Colliod Interface Sci.* **2001**, *243*, 73.

(21) Kelly, S. D.; Kemner, K. M.; Fein, J. B.; Fowle, D. A.; Boyanov, M. I.; Bunker, B. A.; Yee, N. *Geochim. Cosmochim. Acta* **2002**, *66*, 3855.

(22) Templeton, A. S.; Trainor, T. P.; Spormann, A. M.; Newville, M.; Sutton, S. R.; Dohnalkova, A.; Gorby, Y.; Brown, G. E. *Environ. Sci. Technol.* **2003**, *37*, 300.

(23) Griffiths, P. R.; De Haseth, J. A. *Fourier transform infrared spectrometry*; Wiley: New York, 1986.

(24) Gremlich, H.; Yan, B. *Infrared and Raman spectroscopy of biological materials*; Marcel Dekker Inc.: New York, 2000.

(25) Jamin, N.; Dumas, P.; Moncuit, J.; Fridman, W. H.; Teillaud, J. L.; Carr, G. L.; Williams, G. P. *Proc. Natl. Acad. Sci. U.S.A.* **1998**, *95*, 4837.

(26) Holman, H. Y. N.; Goth-Goldstein, R.; Martin, M. C.; Russell, M. L.; McKinney, W. R. *Environ. Sci. Technol.* **2000**, *34*, 2513.

(27) Holman, H. N.; Martin, M. C.; Blakely, E. A.; Bjornstad, K.; McKinney, W. R. *Biopolymers* **2000**, *57*, 329.

(28) Marcelli, A.; Iliescu, C. *Acta Phys. Pol.* **2000**, *100*, 647.

(29) Benning, L. G.; Phoenix, V. R.; Yee, N.; Tobin, M. J. *Geochim. Cosmochim. Acta* **2003**, in press.

(30) Duncan, W. D.; Williams, G. P. *Appl. Opt.* **1983**, *22*, 2914.

(31) Carr, G. L. *Vib. Spectrosc.* **1999**, *19*, 53.

(32) Carr, G. L. *Rev. Sci. Instrum.* **2001**, *72*, 1613.

(33) Phoenix, V. R.; Adams, D. G.; Konhauser, K. O. *Chem.1 Geol.* **2000**, *169*, 329.

(34) Rippka, R.; Deruelles, J.; Waterbury, J. B.; Herdman, M.; Stanier, R. Y. *J. Gen. Microbiol.* **1979**, *111*, 1.

(35) Rushforth, S. R.; Brock, J. T. *Hydrobiologia* **1991**, *224*, 49.

(36) Silva, S. M. F.; Pienaar, R. N. *S. African J. Bot.* **1997**, *63*, 426.

(37) Weckesser, J.; Hofmann, K.; Jürgens, U. J.; Whitton, B. A.; Raffelsberger, B. *J. Gen. Microbiol.* **1988**, *134*, 629.

(38) Lin-vien, D. *The handbook of infrared and Raman characteristic frequencies of organic molecules;* Academic Press: San Diego, 1991.

(39) Naumann, D.; Schultz, C. P.; Helm, D. What Can Infrared Spectroscopy Tell Us about the Structure and Composition of Intact Bacterial Cells? In *Infrared Spectroscopy of Biomolecules*; Mantsch, H. H., Chapman, D., Eds.; Wiley-Liss, Inc.: New York, 1996; p 279.

(40) Naumann, D. FT-Infrared and FT-Raman Spectroscopy in Biomedical Research. In *Infrared and Raman spectroscopy of biological materials*; Gremlich, H., Yan, B., Eds.; Marcel Dekker Inc.: New York, 2000; p 323.

(41) Westall, J. C. *FITEQL, a computer program for determination for chemical equilibrium constants from experimental data,* Version 2.0; Report 82-02; Department of Chemistry, Oregon State University: Corvallis, OR, 1982.

(42) Schrader, M.; Drews, G.; Weckesser, J. *FEMS Microbiol. Lett.* **1981**, *11*, 37.

(43) Weckesser, J.; Katz, A.; Drews, G.; Mayer, H.; Fromme, I. *J. Bacteriol.* **1974**, *120*, 672.

(44) Woitzik, D.; Weckesser, J.; Jürgens, U. J. *J. Gen. Microbiol.* **1988**, *34*, 619.

(45) Beveridge, T. J.; Murray, R. G. E. *J. Bacteriol.* **1976**, *127*, 1502.

(46) Beveridge, T. J.; Koval, S. F. *Appl. and Environ. Microbiol.* **1981**, *42*, 325.

(47) Beveridge, T. J. *Annu. Rev. Microbiol.* **1989**, *43*, 147.

(48) Robbins, R. A.; Bauld, J.; Chapman, D. J. *Cryptogamie Algol* **1998**, *19*, 169.

(49) Cox, J. S.; Smith, D. S.; Warren, L. A.; Ferris, F. G. *Environ. Sci. Technol.* **1999**, *33*, 4515.

(50) Martell, A. E.; Smith, R. M. *Critical stability constants;* Plenum Press: New York, 1974−77.

(51) Pritzer, M.; Weckesser, J.; Jurgens, U. J. *Arch. Microbiol.* **1989**, *153*, 11.

(52) Adhikary, S. P.; Weckesser, J.; Jurgens, U. J.; Golecki, J. R.; Borowiak, D. *J. Gen. Microbiol.* **1986**, *132*, 2595.